Strojniški vestnik - Journal of Mechanical Engineering 64(2018)12, 772-782

DOI:10.5545/sv-jme.2018.5458 Original Scientific Paper
Received for review: 2018-04-25
Received revised form: 2018-07-03
Accepted for publication: 2018-08-09

Buckling Analysis of Axially Functionally Graded Tapered Nanobeams Resting on Elastic Foundations, Based on Nonlocal Elasticity Theory

Ma'en S. Sari[1] – Wael G. Al-Kouz[2,*] – Anas Atieh[3]

[1]German Jordanian University, Mechanical and Maintenance Engineering Department, Jordan
[2]German Jordanian University, Mechatronics Engineering Department, Jordan
[3]German Jordanian University, Industrial Engineering Department, Jordan

The stability analysis of nonlocal axially functionally graded tapered beams has been investigated. Euler-Bernoulli beams at the micro- or nanoscale are modeled using Eringen's nonlocal elasticity theory. The governing equations are derived using the differential constitutive relations, and the Chebyshev collocation method is utilized to convert the differential equation of motion into a set of algebraic equations. Next, the boundary conditions are applied, and the resulting eigenvalue problem is solved to obtain the critical buckling loads. The effects of the Winkler modulus parameter, the shear modulus parameter, the breadth taper ratio, the height taper ratio, the nonlocal scale coefficient, and the boundary conditions on the critical buckling loads have been studied.

Keywords: buckling, axially functionally graded beams, Eringen's nonlocal elasticity theory, Chebyshev collocation method, eigenvalue problem

Highlights

- *The research aims to study the buckling behaviour of axially functionally graded nonlocal nanobeams.*
- *Effects of nonlocal scale parameter, Winkler modulus parameter, the shear modulus parameter, the breadth taper ratio, the height taper ratio, and the boundary conditions were investigated.*
- *The nonlocal elasticity theory and the Chebyshev collocation method were utilized.*
- *It was found that the afore-mentioned parameters have a significant influence on the critical buckling loads.*

0 INTRODUCTION

Micro- and nanoelectromechanical systems have gained appreciable attention for their significant role in many engineering and modern technology fields such as aerospace, nuclear, composites, and electronics due to their excellent mechanical, electrical, and thermal properties in comparison to other structures at the normal (macro) length scale. During manufacturing, producing, assembling, and packaging, some micro- and nanostructures may have geometrical non-uniformities, as variations in the height and the width that may affect the dynamical behaviour of these structures.

For more efficient vibration control, and to provide weight reduction for greater structural efficiency, tapered structures can be used in different engineering applications. Therefore, it is worthwhile to model these non-uniform micro- and nanostructures to predict their dynamical behaviour. Besides, to increase the strength to weight ratio, orthotropic, anisotropic, composite, and functionally graded structures are commonly used in several industrial applications such as civil and aerospace structures. Moreover, the micro- and nanomaterials such as carbon nanotubes and graphene sheets cannot be considered as homogeneous due to the influence of lattice distance or grain size on their mechanical properties.

To ensure that these properties vary smoothly and continuously within the structure, functionally graded (FG) materials, which are made from a mixture of ceramics and metal, can be used, and the properties of these FG materials can be tailored for specific purposes. In contrast, composite materials suffer from premature failure due to the abrupt change in material properties from the matrix to fibre and between the layers [1]. Additionally, these materials may experience the decay in the elastic characteristics as a result of delaminations and chemically unstable medium and lamina adhesives [1]. However, to date, no report has been found in the literature on the buckling behaviour of non-uniform functionally graded nonlocal beams resting on the linear elastic foundation. Motivated by these considerations and to improve the design of MEMS/NEMS, this article aims to study the buckling of nonlocal, double-tapered thin beams resting on elastic foundations.

It is known that the experimental and atomistic simulations and models are capable of showing the influence of the small-scale on the behaviour of micro- or nanostructures; however, these methods are expensive and restricted by computational capacity.

*Corr. Author's Address: German Jordanian University, Mechatronics Engineering Department, Jordan, wael.alkouz@gju.edu.jo

Since the local continuum theories for different structures are scale-free, they are not able to capture the small scale effect on the different properties for structures at the micro- or nanoscale. This makes them inadequate in predicting the dynamical behaviour for these structures [2]. To apply the continuum mechanics approach to the analysis of the micro- and nanostructures, logical and reasonable modifications that take into consideration the scale effect, should be introduced. For this purpose, several theoretical models have been proposed. Among these are the strain gradient theory, the modified coupled stress theory, and the nonlocal elasticity theory [3] and [4] that will be used in this article to carry out the buckling behaviour of nonlocal axially functionally graded Euler-Bernoulli beams resting on elastic foundations.

Calculating natural frequencies and understanding the buckling behaviour are the main issues from a design point of view, since the natural frequencies and the critical buckling loads can be considered to be dynamic properties of a structure. Thus, many researchers have been interested in investigating the free vibration and stability analyses of structures at the nanoscale. For example, Thang et al. [5] illustrated an analytical approach to analyse the nonlinear static buckling of imperfect functionally graded carbon nano-reinforced composite plates subjected to axial compression, for which several linear distributions of the volume fraction of carbon nanotubes were assumed to be graded through the thickness direction according to formulations that are based on Kirchhoff plate theory with Von Karman-type of nonlinearity.

Buckling characteristics of heated FG annular nanoplates resting on an elastic foundation and subjected to various types of thermal loadings were investigated by Ashoori et al. [6]. In their work, an exact analytical solution was introduced for three different types of thermal loadings, and the thermo-mechanical properties for the FG nanoplate were assumed to follow the power law model. The adjacent equilibrium criterion was analyzed by solving the nonlocal stability equations of FG annular. Moreover, a parametric study was conducted to examine the effects of different parameters on the critical buckling temperatures of the size-dependent FG nanoplates. It was concluded that the small-scale effects and thermal loading have a significant effect on thermal stability characteristics of FG annular nanoplates

In the study conducted by Challamel et al. [7], the small length scale effect of microstructured plates was investigated utilizing three different kinds of nonlocal plate theories, namely, the classical stress gradient Eringen's theory, continualization of the discrete lattice model, and the combination of Eringen's model with some additional gradient curvature terms. Analytical solutions for the vibration and buckling of these equivalent continuous systems were obtained, and it was shown that the small length scale coefficient is dependent on the buckling mode and the geometry of the plate. Liu et al. [8] formulated the general equation for transverse vibration of a double-viscoelastic-FGM-nanoplate system with a visco-elastic Pasternak medium in between and each nanoplate subjected to in-plane edge loads based on the Eringen's nonlocal elastic theory and the Kelvin model. Many different factors, such as the structural damping, medium damping, small size effect, loading ratio, and Winkler modulus and shear modulus of the medium are included in the general equation. It was illustrated that the vibrational frequency of the system for the out-of-phase vibration is dependent on different factors, such as structural damping, small size effect and viscoelastic Pasternak medium, and it was found that the buckling load of the system for the in-phase buckling case is independent of the viscoelastic Pasternak medium. It was concluded that the buckling load for the out-of-phase case is a function of the small size effect, loading ratio, and Pasternak medium.

Golmakani and Rezatalab [9] analysed the non-uniform biaxial buckling analysis of an orthotropic single-layered graphene sheet embedded in a Pasternak elastic medium using the nonlocal Mindlin plate theory. All edges of the sheet were subjected to linearly varying normal stresses. The governing equations were derived based on first-order shear deformation theory, and the differential quadrature method was used to solve the governing equations for various boundary conditions. Effects of scale, aspect ratio, polymer matrix properties, type of planar loading, mode numbers, and boundary conditions were discussed in details. Taati [10] utilized the differential operator method to investigate the buckling and post-buckling behaviour of uniform functionally graded microbeams subjected to axial compressive force and thermal loading. It was assumed that the beams were resting on an elastic foundation. The modified couple stress theory and the principle of minimum potential energy were used to derive the governing equations. Moreover, Ebrahimi and Barati [12] applied the nonlocal strain gradient theory to examine the buckling behaviour of axially functionally graded nanobeams resting on a variable elastic medium. Hamilton's principle was used to obtain the governing equations, and a Galerkin-based solution was implemented to obtain

the buckling loads. Ebrahimi et al. [12] carried out the vibrational and buckling behaviour of nanotubes utilizing Eringen's nonlocal elasticity theory and considering the surface effects. The governing equation was derived using Hamilton's principle, and the natural frequencies, as well as the buckling loads, were obtained by applying the differential transform method. Latifi et al. [13] investigated the buckling problem of thin rectangular functionally graded plates subjected to proportional biaxial compressive loadings with arbitrary edge supports. The classical plate theory based on the physical neutral plane was applied, and the displacement function was considered to be in the form of a double Fourier series. The effects of the plate aspect ratio, the loading proportionality factor on the buckling load of the plate with different common boundary conditions were studied.

Pradhan and Murmu [14] implemented the nonlocal elasticity theory to study the buckling behaviour of single-layered graphene sheets embedded in an elastic medium modelled by Winkler-type and Pasternak-type foundations. The governing differential equations based on the principle of virtual work were derived. It was shown that the buckling loads are strongly dependent on the small-scale coefficients and the stiffness of the surrounding elastic medium. Shahidi et al. [15] developed a nonlocal continuum model based on Eringen's theory for vibration analysis of orthotropic nanoplates (modelled as Kirchhoff plates) with arbitrary variation in thickness. The variational principle and Ritz functions were employed, and the effect of thickness variation on natural frequencies was investigated for different nonlocal parameters, mode numbers, geometries and boundary conditions.

Moreover, Asbaghian Namin and Pilafkan [16] investigated the free vibration of defective graphene sheets via nonlocal elasticity theory, and the first-order shear deformation was used to derive the governing equations, which were solved using a generalized differential quadrature method. It was shown that the shapes and distributions of the structural defects, the number of missing atoms, and the vacancy defect reconstruction have a noticeable effect on the natural frequencies of the graphene sheets. Zhang et al. [17] applied the nonlocal elasticity theory to carry out the vibration behaviour of quadrilateral single-layered graphene sheets (modelled as Kirchhoff plates) in a magnetic field. The governing equations were solved by employing the element-free kp-Ritz method. The effects of the skew angles, nonlocal parameter, the magnetic field, and the boundary conditions on the fundamental frequencies of the single-layered graphene sheets were discussed.

Furthermore, Li and Hu [18] studied the free torsional vibration behaviour of tubes made of a bi-directional functionally graded material. It was assumed that the material properties of the nanotube vary in the length direction according to an exponential distribute function and in the radius direction according to a power-law function. It was concluded that the torsional frequencies are increased by decreasing nonlocal parameters, and it was observed that this parameter does not affect the mode shapes of the nanotubes. The vibration formulation for a nanoscaled beam embedded in an elastic matrix under the effect of thermal environments was presented by Demir and Civalek [19]. The governing equations were obtained using Hamilton's principle, the variational approach, and the nonlocal elasticity theory. A new Finite element method was utilized to solve for the vibrational frequencies that were affected by the Pasternak foundation parameter, the small-scale parameter, and the thermal effect.

Additionally, Murmu and Adhikari [20] considered the nonlocal vibration of a double-nanoplate-system bonded by an elastic medium. Closed form solutions were obtained for the natural frequencies of a nonlocal double-nanoplate-system. It was concluded that the increase of the stiffness of the coupling springs in the system reduces the small-scale effects during the asynchronous modes of vibration.

In the present article, Eringen's nonlocal elasticity theory is utilized to study the small-scale effect on the buckling behaviour of axially functionally graded (AFG) tapered Euler-Bernoulli beams resting on an elastic foundation. The governing equation is derived using Eringen's nonlocal constitutive relations along with Hamilton's principle. The Chebyshev spectral collocation method is applied to transform the governing differential equation into a system of algebraic equations, and then the resulted eigenvalue problem is solved to obtain the natural frequencies and the critical buckling loads. In this study, the variable height, breadth, cross-sectional area, second moment of area, mass density, and Young's modulus will be presented as the variable coefficients of the governing differential equation. It is believed that the results of this study can be used for the design and optimization of double-tapered nanodevices made of axially functionally graded materials and are embedded in elastic medium, and may help in studying the buckling response of double-tapered nanodevices (that can be modeled as thin beams) when

used as mechanical resonators, sensors, actuators, and vibrating components.

1 THEORY

1.1 Chebyshev Spectral Collocation

The Chebyshev points are the points that represent the projections on the interval $[-1,1]$ of equally spaced points of a unit circle. These points are given as **[21]**:

$$x_j = \cos\left(j\pi / N\right), \quad j = 0,1,...,N. \tag{1}$$

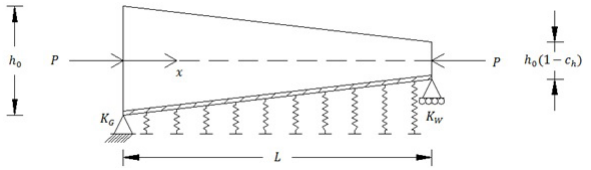

Fig. 1. *Nonlocal AFG tapered Euler-Bernoulli beam resting on Elastic foundation and subjected to a constant axial compressive load*

The Chebyshev differentiation Matrix DN of size $(N+1)\times(N+1)$ can be obtained by interpolating a Lagrange polynomial of degree N at each Chebyshev point, differentiating the polynomial, and then finding its derivative at each Chebyshev point. The entries of the D_N matrix are found in **[21]**. The Chebyshev collocation method can be used to solve ordinary or partial differential equations by representing the n^{th} derivative of a function by $Dn=(D_N)^n$.

2.2 Nonlocal Theory

At the macro scale, the stress at a point in a body depends on the strain at the same point. However, in the nonlocal elasticity theory pioneered by Eringen **[3]**, the stress at a point in an elastic domain is related to the stress field at all points in the domain. Eringen's theory is based on the atomic theory of lattice dynamics and experimental results on phonon scattering and dispersion **[3]**.

The stress tensor t_{ij} is defined for nonlocal linear elastic solids as **[3]**:

$$t_{ij} = \int_V \alpha\left(|x'-x|\right)\sigma_{ij}\left(x'\right)dV\left(x'\right), \tag{2}$$

where x is a reference point in the elastic domain, $\alpha(|x'-x|)$ is the non-local kernel attenuation function which introduces the nonlocal effects at the reference point x produced by the local stress σ_{ij} at any point x', and $|x'-x|$ is the Euclidean form of the distance. Eringen **[3]** introduced a linear differential operator ς, defined by $\varsigma=1-(e_0l)^2\nabla^2$, where e_0 is a material constant estimated by experiments, simulations, or other models and theories. In Eringen's analysis, the value of e_0 was taken to be 0.39. Furthermore, the constant l represents the characteristic internal length which (for structures at the nanoscale) is of the same order of the external length. The Laplace operator ∇^2 is given as:

$$\nabla^2 = \frac{\partial^2}{\partial x^2}. \tag{3}$$

According to Eringen **[3]**, the integral constitutive relation of Eq. (3) could be simplified to the following form **[4]**:

$$\left(1-\left(e_0l\right)^2\nabla^2\right)t_{ij} = \sigma_{ij}. \tag{4}$$

Due to its simple form, Eq. (4) has been used by many researchers in applying the nonlocal theory to study and analyze the buckling, vibration, and mechanics of micro- and nanostructures.

Fig. 1. shows a Euler-Bernoulli beam resting on an elastic foundation and subjected to a constant compressive force P. The governing differential equation of motion for this system is given by **[22]** and **[23]**:

$$\frac{d^2}{dx^2}\left[E\left(x\right)I\left(x\right)\frac{d^2\hat{w}}{dx^2}\right] + P\frac{d^2\hat{w}}{dx^2} + k_w\hat{w} - k_G\frac{d^2\hat{w}}{dx^2} = 0, \tag{5}$$

where x is the spatial coordinate, $\hat{w}$ is the transverse deflection, $I(x)$ is the beam's area moment of inertia of the cross-section, $E(x)$ is Young's modulus of Elasticity, and k_w and k_G are the Winkler modulus and the shear modulus parameters of the surrounding medium, respectively.

For a Euler-Bernoulli beam, the bending moment is given as:

$$M\left(x\right) = -E\left(x\right)I\left(x\right)\frac{d^2\hat{w}}{dx^2}. \tag{6}$$

In light of Eq. (5), $d^2\mathrm{M}\left(\hat{x}\right)/d\hat{x}^2$ is given by:

$$\frac{d^2M}{dx^2} = P\frac{d^2\hat{w}}{dx^2} + k_w\hat{w} - k_G\frac{d^2\hat{w}}{dx^2}. \tag{7}$$

From Eq. (5) and utilizing Hooke's law, the constitutive relation for the moment $M\left(\hat{x},\hat{t}\right)$ is given as:

$$M\left(x\right) - \left(e_0a\right)^2\frac{d^2M}{dx^2} = -E\left(x\right)I\left(x\right)\frac{d^2\hat{w}}{dx^2}. \tag{8}$$

Inserting Eq. (8) into Eq. (7), yields:

$$M(x)=(e_0a)^2\left[P\frac{d^2\hat{w}}{dx^2}+k_w\hat{w}-k_G\frac{d^2\hat{w}}{dx^2}\right]-E(x)I(x)\frac{d^2\hat{w}}{dx^2}. \quad (9)$$

Substituting Eq. (9) into Eq. (6), the equation of the transverse motion of the nonlocal Euler-Bernoulli beam resting on an elastic foundation and subjected to a constant compressive force is given as:

$$(e_0a)^2\left[P\frac{d^2\hat{w}}{dx^2}+k_w\hat{w}-k_G\frac{d^2\hat{w}}{dx^2}\right]-E(x)I(x)\frac{d^2\hat{w}}{dx^2}-(e_0a)^2\left[(e_0a)^2\left(P\frac{d^4\hat{w}}{dx^4}+k_w\frac{d^2\hat{w}}{dx^2}-k_G\frac{d^4\hat{w}}{dx^4}\right)\right]+(e_0a)^2\frac{d^2}{dx^2}\left[E(x)I(x)\frac{d^2\hat{w}}{dx^2}\right]=-E(x)I(x)\frac{d^2\hat{w}}{dx^2}. \quad (10)$$

Simplifying and collecting terms yields:

$$\frac{d^2}{dx^2}\left[E(x)I(x)\frac{d^2\hat{w}}{dx^2}\right]+P\frac{d^2\hat{w}}{dx^2}-(e_0a)^2P\frac{d^4\hat{w}}{dx^4}+k_w\hat{w}-k_G\frac{d^2\hat{w}}{dx^2}-(e_0a)^2k_w\frac{d^2\hat{w}}{dx^2}+(e_0a)^2k_G\frac{d^4\hat{w}}{dx^4}=0. \quad (11)$$

In the present study, $E(x)$ and $I(x)$ are given as [22]:

$$E(x)=E_0\left(1+\frac{x}{L}\right),\ I(x)=I_0\left(1-c_b\frac{x}{L}\right)\left(1-c_h\frac{x}{L}\right)^3, \quad (12)$$

where E_0 and I_0 are respectively the modulus of elasticity, and area moment of inertia at $x=0$, c_b is the breadth taper ratio, and c_h is the height taper ratio. To obtain the normalized equations, the dimensionless parameters are introduced as:

$$X=\frac{x}{L},\quad W=\frac{\hat{w}}{L},\quad \mu=\frac{e_0a}{L},\quad \lambda=\frac{PL^2}{E_0I_0},\quad K_W=\frac{k_wL^4}{E_0I_0},\quad K_G=\frac{k_GL^2}{E_0I_0},\quad E(X)=\frac{E(x)}{E_0},\quad I(X)=\frac{I(x)}{I_0}. \quad (13)$$

Substituting Eq. (13) into Eq. (11) and rearranging, yields:

$$\frac{d^2}{dX^2}\left(E(X)I(X)\frac{d^2W}{dX^2}\right)+K_wW-K_G\frac{d^2W}{dX^2}-\mu^2K_w\frac{d^2W}{dX^2}+\mu^2K_G\frac{d^4W}{dX^4}=\lambda\left(-\frac{d^2W}{dX^2}+\mu^2\frac{d^4W}{dX^4}\right). \quad (14)$$

The critical buckling loads are determined by solving Eq. (14) as an eigenvalue problem.

2 SOLUTION PROCEDURE

The Chebyshev spectral collocation method is used to discretize the governing equation and the boundary conditions. It is known that for structures modelled as Euler-Bernoulli beams, two boundary conditions should be satisfied at the edges of the beam, and as there is only one unknown at each point $W_{i,j}$, therefore, the Chebyshev collocation method can be applied to satisfy one boundary condition only. To overcome this difficulty, the boundary conditions are applied by expressing the displacement at the boundary point and its adjacent point in terms of the displacement at other points in the domain. For example, the boundary conditions of a beam with clamped ends are given as:

$$W(0)=\frac{\partial W(0)}{\partial X}=W(1)=\frac{\partial W(1)}{\partial X}=0. \quad (15)$$

Applying the Chebyshev collocation method, these conditions are expressed as:

$$W_1=0,$$

$$D^1_{1,1}W_1+D^1_{1,2}W_2+D^1_{1,N}W_N+D^1_{1,N+1}W_{N+1}=-\sum_{k=3}^{N-1}D^1_{1,k}W_k,$$

$$W_{N+1}=0,$$

$$D^1_{N+1,1}W_1+D^1_{N+1,2}W_2+D^1_{N+1,N}W_N+D^1_{N+1,N+1}W_{N+1}=-\sum_{k=3}^{N-1}D^1_{N+1,k}W_k. \quad (16)$$

As the X-axis is normalized to be in the range of $[0,1]$, the original Chebyshev points are shifted to be in this interval. Accordingly, the Chebyshev differentiation matrices will have different entries than those obtained by Trefethen [21], as they depend on the distribution of the points.

Eq. (16) is written in matrix-vector form as:

$$\begin{bmatrix}D^1_{1,2} & D^1_{1,N}\\ D^1_{N+1,2} & D^1_{N+1,N}\end{bmatrix}\begin{Bmatrix}W_2\\ W_N\end{Bmatrix}=\begin{Bmatrix}-\sum_{k=3}^{N-1}D^1_{1,k}W_k\\ -\sum_{k=3}^{N-1}D^1_{N+1,k}W_k\end{Bmatrix}. \quad (17)$$

From Eq. (17), the displacements at the points adjacent to the boundaries are given as:

$$\begin{Bmatrix}W_2\\ W_N\end{Bmatrix}=\frac{1}{Det}\begin{bmatrix}D^1_{N+1,N} & D^1_{1,N}\\ D^1_{N+1,2} & D^1_{1,2}\end{bmatrix}\begin{Bmatrix}-\sum_{k=3}^{N-1}D^1_{1,k}W_k\\ -\sum_{k=3}^{N-1}D^1_{N+1,k}W_k\end{Bmatrix}, \quad (18)$$

where *Det* is the determinant of the 2 × 2 matrix in the left side of Eq. (18) and is given by:

$$Det = \left(D^1_{1,2} \times D^1_{N+1,N}\right) - \left(D^1_{1,N} \times D^1_{N+1,2}\right). \quad (19)$$

From Eq. (18), the displacements W_2 and W_N are written in terms of the displacements at the other points as:

$$W_2 = \frac{1}{Det}\left(-D^1_{N+1,N}\sum_{k=3}^{N-1} D^1_{1,k}W_k + D^1_{1,N}\sum_{k=3}^{N-1} D^1_{N+1,k}W_k\right), \quad (20)$$

$$W_N = \frac{1}{Det}\left(D^1_{N+1,2}\sum_{k=3}^{N-1} D^1_{1,k}W_k - D^1_{1,2}\sum_{k=3}^{N-1} D^1_{N+1,k}W_k\right). \quad (21)$$

As a result, the Chebyshev collocation matrices are modified as:

$$\begin{aligned}\bar{D}^n_{i,k} &= \sum_{k=3}^{N-1} D^n_{i,k} \\ &+ D^n_{i,2}\frac{1}{Det}\left(-D^1_{N+1,N}\sum_{k=3}^{N-1} D^1_{1,k} + D^1_{1,N}\sum_{k=3}^{N-1} D^1_{N+1,k}\right) \\ &+ D^n_{i,N}\frac{1}{Det}\left(D^1_{N+1,2}\sum_{k=3}^{N-1} D^1_{1,k} - D^1_{1,2}\sum_{k=3}^{N-1} D^1_{N+1,k}\right)\end{aligned}$$

$$\text{for } i = 3,4,\ldots N-1. \quad (22)$$

The boundary conditions of a beam with simply supported ends are given as:

$$W(0) = \frac{\partial^2 W(0)}{\partial X^2} = W(1) = \frac{\partial^2 W(1)}{\partial X^2} = 0. \quad (23)$$

In this case, the boundary conditions are expressed using the Chebyshev collocation method as in Eq. (16), except that each differentiation matrix D^1 is substituted with the differentiation matrix D^2. Eq. (14) is discretized by the Chebyshev collocation method as:

$$\begin{aligned}&\left(\begin{aligned}&\left(R1\times\bar{D}^2\right)+\left(R2\times\bar{D}^3\right)+\left(R3\times\bar{D}^4\right)\\&+K_W I - K_G\bar{D}^2 - \mu^2 K_W\bar{D}^2 + \mu^2 K_G\bar{D}^4\end{aligned}\right)\{W\} = \\ &\lambda\left(-\bar{D}^2 + \mu^2\bar{D}^4\right)\{W\}, \end{aligned} \quad (24)$$

where I is a $(M-4)\times(M-4)$ identity matrix, $R1$, $R2$, and $R3$ are diagonal $(M-4)\times(M-4)$ matrices with values of $R1_i$, $R2_i$ and $R3_i$ on the main diagonal, respectively, where:

$$\begin{aligned}R1_i &= \left(2c_b\left(c_h x_i - 1\right)^3\right) \\ &+ \left(6c_h\left(c_b + 2c_b x_i - 1\right)\left(c_h x_i - 1\right)^2\right) \\ &+ \left(6c_h^2\left(1+x_i\right)\left(1-c_b x_i\right)\left(1-c_h x_i\right)\right),\end{aligned} \quad (25)$$

$$\begin{aligned}R2_i &= \left(2\left(c_b - 2c_b x_i - 1\right)\left(c_h x_i - 1\right)^3\right) \\ &+ \left(6c_h\left(1+x_i\right)\left(1-c_b x_i\right)\left(1-c_h x_i\right)\left(c_h x_i - 1\right)\right),\end{aligned} \quad (26)$$

$$R3_i = \left(1+x_i\right)\left(1-c_b x_i\right)\left(1-c_h x_i\right)\left(c_h x_i - 1\right)^2, \quad (27)$$

3 RESULTS AND DISCUSSION

There are no results for the critical buckling loads for micro- or nanoaxially functionally graded non-uniform Euler-Bernoulli beams resting on elastic foundations and subjected to constant axial compressive forces based on the nonlocal elasticity theory. Thus, for validation purpose, the comparison is made with local AFG non-uniform Euler-Bernoulli that are not embedded in the elastic medium, by setting the scale effect, the Winkler modulus parameter, and the shear modulus parameter to zero. To demonstrate the accuracy of the results obtained from the proposed technique, the critical buckling loads of local orthotropic non-uniform AFG Euler-Bernoulli beams with simply supported and clamped edges are compared with those obtained by Shahba and Rajasekaran [22]. The notation S-S denotes a beam that is simply supported at both edges, whereas the notation C-C denotes a beam with clamped edges. To show the stability and the accuracy of the proposed technique, a convergence study is conducted for the non-dimensional critical loads of local AFG beams with simply supported and clamped edges. From Table 1, it can be observed that the sufficient number of points to attain accurate results is N=10 for S-S beams, and N=12 for C-C beams.

Table 1. Convergence of Non-dimensional critical load for AFG S-S and C-C tapered beams, ($c_h = c_b$ = 0.2, $\mu = K_w = K_G$ = 0)

	S-S	C-C		S-S	C-C
N=7	9.5876	38.0371	N=11	9.5971	37.6022
N=8	9.5979	37.5838	N=12	9.5971	37.6023
N=9	9.5976	37.5967	N=13	9.5971	37.6023
N=10	9.5971	37.6020	Ref. [38]	9.5971	37.6023

As shown in Tables 2 and 3, it is clear that the results of the proposed model are in good agreement with those obtained by Shahba and Rajasekaran [22]. Additionally, the generated results for an isotropic and uniform S-S nonlocal beam (not embedded in an elastic medium) are compared to those obtained by Reddy [24], as shown in Table 4. Very good agreement is noted, and these tables reflect the validity of the proposed model and solution.

Table 2. *Non-dimensional critical load ($\lambda = P_{cr}L^2 / E_0I_0$) for an AFG C-C tapered beam*

c_h	c_b	0	0.2	0.8
0	Present Study	57.3940	51.7856	30.8922
	Ref. [22]	57.3940	51.7856	30.8922
0.2	Present Study	41.9169	37.6023	21.6802
	Ref. [22]	41.9169	37.6023	21.6802
0.4	Present Study	28.1794	25.0890	13.8242
	Ref. [22]	28.1794	25.0890	13.8242
0.6	Present Study	16.3412	14.3958	7.4275
	Ref. [22]	16.3412	14.3958	7.4275
0.8	Present Study	6.6801	5.7836	2.6649
	Ref. [22]	6.6801	5.7836	2.6649

Table 3. *Non-dimensional critical load ($\lambda = P_{cr}L^2 / E_0I_0$) for an AFG S-S tapered beam*

c_h	c_b	0	0.2	0.8
0	Present Study	14.5112	13.1398	8.3957
	Ref. [22]	14.5112	13.1398	8.3957
0.2	Present Study	10.6860	9.5971	5.8498
	Ref. [22]	10.6860	9.5971	5.8498
0.4	Present Study	7.2831	6.4715	3.7019
	Ref. [22]	7.2831	6.4715	3.7019
0.6	Present Study	4.3287	3.7892	1.9748
	Ref. [22]	4.3287	3.7892	1.9748
0.8	Present Study	1.8667	1.5950	0.7075
	Ref. [22]	1.8667	1.5950	0.7075

Table 4. *Comparison of the Buckling loads with Reddy [24] for an isotropic S-S uniform beam*

μ	Present Study	Ref. [24]
0	9.8696	9.8696
$0.5^{½}$ / 10	9.4055	9.4055
$1.0^{½}$ / 10	8.9830	8.9830
$1.5^{½}$ / 10	8.5969	8.5969
$2.0^{½}$ / 10	8.2426	8.2426
$2.5^{½}$ / 10	7.9163	7.9163
$3.0^{½}$ / 10	7.6149	7.6149
$3.5^{½}$ / 10	7.3356	7.3356
$4.0^{½}$ / 10	7.0761	7.0761
$4.5^{½}$ / 10	6.8343	6.8343
$5.0^{½}$ / 10	6.6085	6.6085

Variations of the dimensionless critical buckling loads at different values of the scale parameter of AFG nano C-C and S-S beams with $c_b = c_h = 0.2$, $K_G = 10$ and $K_W = 200$ are presented in Fig. 2. The scale parameter is taken in the range of 0 to 1. It is observed that as the scale parameter increases, the buckling loads decrease. The rate at which the buckling loads decrease is higher for the AFG nano C-C beams than that for the AFG nano S-S beams. Additionally, as shown in the figure, the dimensionless buckling loads for the AFG C-C and S-S nanobeams have the same value for $\mu > 0.2$.

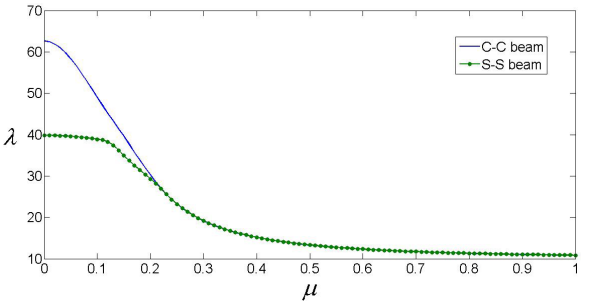

Fig. 2. *Variation of the critical buckling load with the nonlocal parameter of a C-C and S-S AFG Euler Bernoulli beam ($c_b = c_h = 0.2$, $K_G = 10$, $K_W = 200$)*

Fig. 3 shows the effect of the breadth taper ratio (c_b) on the critical dimensionless buckling loads of AFG C-C and S-S beams with $c_h = 0.2$, $K_G = 10$ and $K_W = 200$. The breadth taper ratio is taken in the range of 0 to 0.8. It is observed that as the value of $c_b$increases, the buckling load decreases, and the buckling load of the AFG C-C beam is more sensitive to the increase in c_b than the buckling load of the AFG S-S beam. For $\mu = 0$, it is noticed from Fig. 3a that as c_b increases from 0 to 0.8, the buckling load of the AFG C-C beam decreases from 66.98 to 46, whereas for the AFG S-S beam, it decreases from 40.95 to 33.65. In Fig. 3b, the effect of the breadth ratio (c_b) on the critical dimensionless buckling loads of AFG C-C and S-S nonlocal beams with $c_h = 0.2$, $K_G = 10$, $K_W = 200$, and $\mu = 0.1$ is presented. As observed from Fig. 3, the increase in c_b has a greater influence on the dimensionless buckling load of the AFG C-C nonlocal beams than that on the dimensionless buckling load of the AFG S-S nonlocal beams. Moreover, as c_b increases, the difference between the dimensionless buckling loads for the AFG C-C and S-S nanobeams becomes smaller.

The variations of the dimensionless critical buckling loads at different values of the height taper ratio (c_h) of AFG C-C and S-S beams with $c_b = 0.2$, $K_G = 10$ and $K_W = 200$ are presented in Fig. 4a. As for the breadth taper ratio, the height taper ratio is taken in the range of 0 to 0.8. The figure reveals that the critical buckling load decreases as the value of c_h increases, and the buckling load of the AFG C-C beam is more sensitive to the increase in c_h than that of the AFG S-S beam. The figure shows that as $c_h$increases from 0 to 0.8, the buckling load of the AFG C-C beam decreases

from 76.8 to 22.79, whereas for the AFG S-S beam, it decreases from 43.33 to 17.68. The effect of c_h on the critical dimensionless buckling loads of AFG C-C and S-S nonlocal beams with c_b=0.2, K_G=10, K_W=200 and μ=0.1 is shown in Fig. 4b. It is noticed that as c_h increases from 0 to 0.58, the difference between the dimensionless buckling loads for the AFG C-C and S-S nanobeams becomes smaller, and for c_h>0.58, the critical buckling loads for the AFG C-C and S-S nanobeams are equal.

Fig. 5a shows the effect of shear modulus parameter (K_G) on the critical dimensionless buckling load of an axially functionally graded S-S and C-C beams with c_b=c_h=0.2, K_W=200 and μ=0. It is observed that as the value of the shear modulus parameter increases, the critical buckling load increases, and the buckling load for the C-C beam is higher than that for the S-S beam for the same value of K_G. However, the rate at which the buckling load increases with K_G is higher for the S-S beam. For example, as K_G increases from 0 to 10, the increasing rate of the buckling load is 33 % for the S-S beam and 19 % for the C-C beam. In Fig. 5b, the effect of K_G on the buckling load with c_b=c_h=0.2, K_W=200, and μ=0.1 is presented. As in Fig. 5a, the figure reveals that the buckling load increases as K_G increases, however, the increasing rate is smaller than that when μ=0. Furthermore, it is observed that the buckling load of the AFG C-C nanobeams is more affected by the increase of the scale parameter than that for the AFG S-S nanobeams. For instance, at K_G=0, the buckling load for the AFG C-C nanobeam decreases from 53 to 38 as the scale parameter increases from 0 to 0.1, whereas for the AFG S-S nanobeam it decreases from 30 to 28 as the scale parameter increases from 0 to 0.1.

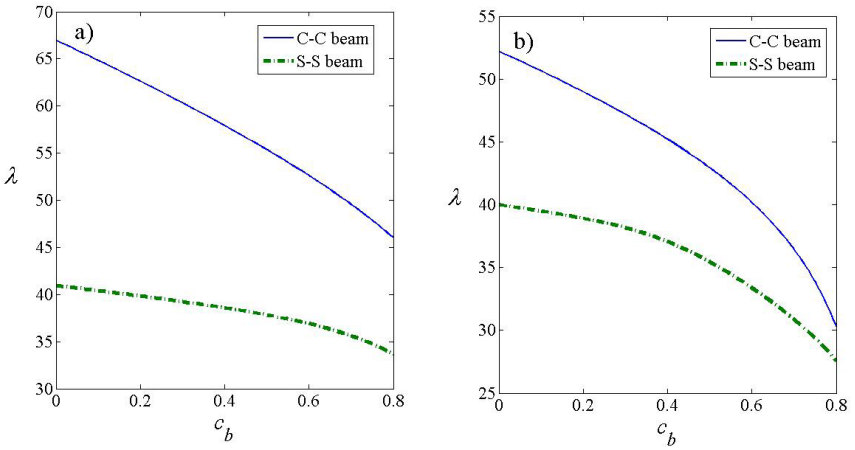

Fig. 3. *Variation of the critical buckling load with the breadth ratio of a C-C and S-S AFG Euler-Bernoulli beam (c_h = 0.2, K_G = 10, K_W = 200; a) μ = 0, and b) μ = 0.1)*

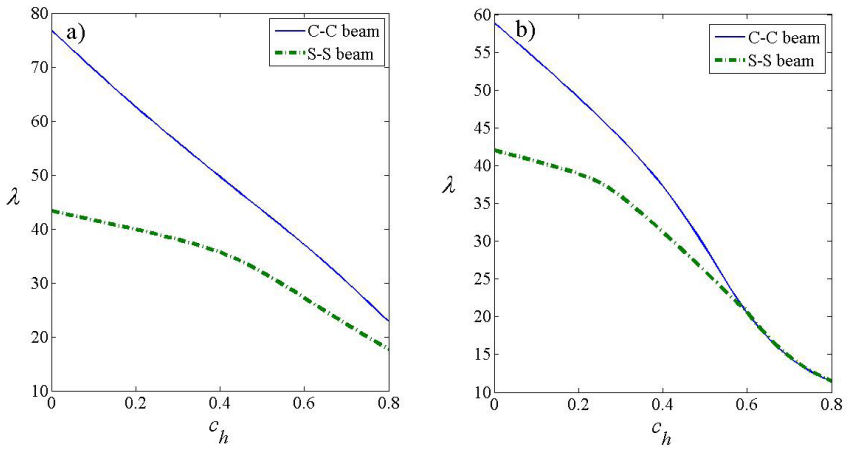

Fig. 4. *Variation of the critical buckling load with the height ratio of a C-C and S-S AFG Euler-Bernoulli beam (c_b = 0.2, K_G = 10, K_W = 200; a) μ = 0, and b) μ = 0.1)*

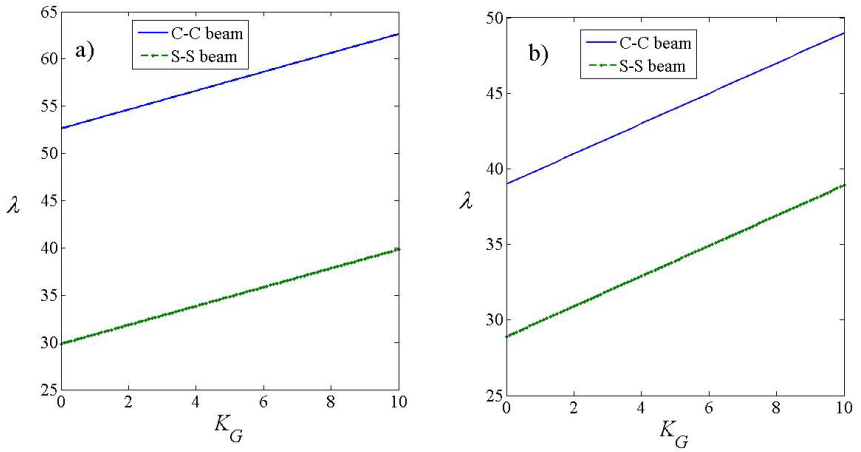

Fig. 5. *Variation of the critical buckling load with shear modulus parameter of a C-C and S-S AFG Euler-Bernoulli beam ($c_b = c_h = 0.2$, $K_W = 200$; a) $\mu = 0$, and b) $\mu = 0.1$)*

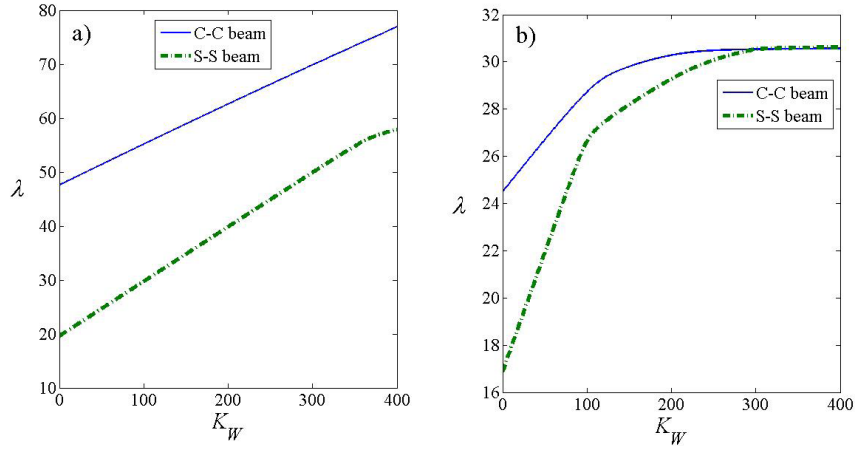

Fig. 6. *Variation of the critical buckling load with Winkler modulus parameter of a C-C and S-S AFG Euler-Bernoulli beam ($c_b = c_h = 0.2$, $K_G = 10$; a) $\mu = 0$, and b) $\mu = 0.2$)*

Fig. 6a shows the effect of the Winkler modulus parameter (K_W) on the critical dimensionless buckling loads of AFG C-C and S-S nonlocal beams with c_b=c_h=0.2, K_G=10 and μ=0. The Winkler modulus parameter is taken in the range of 0 to 400. Similar values of modulus parameter were taken by Pardhan and Murmu [14]. It is concluded that as the value of K_W increases, the buckling load linearly increases with a constant slope, and the increasing rate for the dimensionless buckling load of the AFG S-S nonlocal beams is greater than that of the AFG C-C nonlocal beams. In Fig. 6b, the effect of the Winkler modulus parameter (K_W) on the critical dimensionless buckling loads of AFG C-C and S-S nonlocal beams with c_b=c_h=0.2, K_G=10 and μ=0.2 is presented. The figure reveals that the increasing rate of the dimensionless buckling load depends on the range of the Winkler modulus parameter. For example, for the AFG S-S nonlocal beam, the increasing rate of the dimensionless buckling load is approximately 59 % as K_W increases from 0 to 104, 14 % as K_W increases from 104 to 296, and only 0.4 % as K_W increases from 296 to 400. Similar observations can be made for the AFG C-C nonlocal beams. A point of interest is that the dimensionless buckling loads for the S-S and C-C beams become equal to each other for K_W>296.

For a more general view, three-dimensional plots are shown in Figs. 7 and 8. In Fig. 7, the dimensionless critical buckling loads of the AFG S-S nanobeams with c_b=c_h=0.2, and K_G=10, are plotted versus the nonlocal scale parameter and the Winkler modulus parameter. It is shown that as the scale parameter increases, the rate at which the dimensionless critical buckling load increases with the Winkler modulus

parameter becomes smaller. For example, at $\mu=0$, the dimensionless critical buckling load of the S-S nanobeams increases from 19.6 to 57.78 as K_W increases from 0 to 400. On the other hand, at $\mu=1$, the dimensionless critical buckling load increases from 10.82 to 10.86 as K_W increases from 0 to 400. This leads us to conclude that the scale parameter is more dominant than the Winkler modulus parameter, and at relatively high values of the nonlocal scale parameter, the value of the Winkler modulus parameter has a negligible influence on the dimensionless critical buckling loads.

In Fig. 8, the dimensionless critical buckling loads of the AFG S-S nanobeam with $c_h=0.2$, $K_W=300$ and $K_G=5$, are plotted versus the nonlocal scale parameter and the breadth taper ratio (c_b). The figure reveals that the dimensionless critical buckling loads decrease with the increase in the nonlocal scale parameter and the breadth taper ratio.

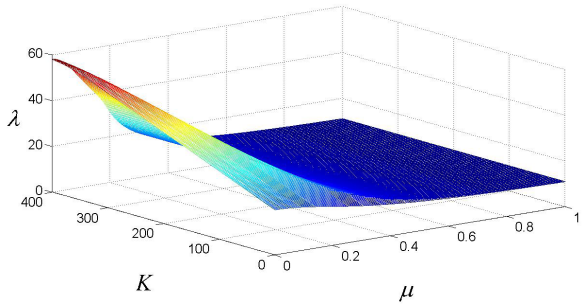

Fig. 7. *Variation of the critical buckling load of a nonlocal AFG S-S Euler-Bernoulli beam with the nonlocal parameter and Winkler modulus parameter ($c_b=c_h=0.2$, $K_G=10$)*

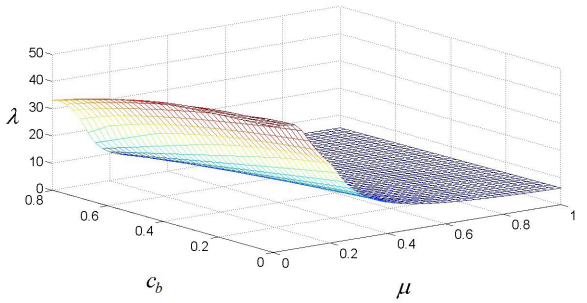

Fig. 8. *Variation of the critical buckling load of a nonlocal AFG S-S Euler-Bernoulli beam with the nonlocal parameter and the breadth taper ratio ($c_h=0.2$, $K_G=5$, $K_W=300$)*

4 CONCLUSIONS

The buckling behaviour of nonlocal axially functionally graded tapered Euler-Bernoulli beams embedded in the elastic medium was performed. Eringen's nonlocal elasticity theory was used to derive the governing equation of motion. The Chebyshev spectral collocation method was utilized, and the boundary conditions were applied by expressing the displacements at the boundaries and their adjacent points in terms of the displacements at all other points in the domain, and then the resulting eigenvalue problem was solved to obtain the critical buckling loads. The effects of the nonlocal scale coefficient, the Winkler modulus parameter, the shear modulus parameter, breadth taper ratio, height taper ratio, and the boundary conditions on the critical buckling loads were studied. It was observed that the nonlocal scale parameter has a significant effect on the critical buckling loads, and the results reveal that beams with clamped ends are more affected by the scale parameter. In general, the critical buckling loads for the C-C beams are higher than those for the S-S beams; however, at relatively high values of the nonlocal scale parameter, the values of the critical buckling loads are very close to each other. It is concluded that the critical buckling load diminishes due to the rise of the nonlocal parameter, and the breadth and height taper ratios. In contrast, the critical buckling load increases as the shear modulus and Winkler modulus parameters become larger.

The authors hope that the obtained results may be useful for scientists in designing and working on the micro- or nanoaxially functionally graded thin structures.

5 NOMENCLATURE

c_b breadth taper ratio,
c_h hight taper ratio,
D_N Chebyshev differentiation matrix,
$E(x)$ modulus of elasticity, [N/ m^2]
$e_o l$ nonlocal parameter, [m]
$I(x)$ moment of inertia of the beam, [m^4]
k_G shear modulus parameter, [N]
K_G non-dimensional Shear modulus parameter,
k_w winkler modulus parameter, [N/ m^2]
K_W non-dimensional Winkler modulus parameter,
L length of the beam, [m]
$N+1$ number of Chebyshev points,
P compressive constant axial load, [N]
t_{ij} stress tensor, [N/ m^2]
w transverse displacement, [m]
W non-dimensional transverse displacement,
x Cartesian coordinate, [m]
X non-dimensional Cartesian coordinate,

Greek Symbols

λ non-dimensional critical load,

μ non-dimensional nonlocal parameter,
ζ differential operator,
σ_{ij} local stress, [N/ m^2]

6 REFERENCES

[1] Natarajan, S., Ferreira, A.J.M., Bordas, S., Carrera, E., Cinefra, M., Zenkour, A.M. (2014). Analysis of functionally graded material plates using triangular elements with cell-based smoothed discrete shear gap method. *Mathematical Problems in Engineering*, art. ID 247932, **DOI:10.1155/2014/247932**.

[2] Wang, C.M., Zhang, Y.Y., He, X.Q. (2007). Vibration of nonlocal Timoshenko beams. *Nanotechnology*, vol. 18, no. 10, p. 105401, **DOI:10.1088/0957-4484/18/10/105401**.

[3] Eringen, A.C. (2002). *Nonlocal Continuum Field Theories*. Springer-Verlag, New York, **DOI:10.1007/b97697**.

[4] Eringen, A.C. (1983). On differential equations of nonlocal elasticity and solutions of screw dislocation and surface waves. *Journal of Applied Physics*, vol. 54, no. 9, p. 4703-4710, **DOI:10.1063/1.332803**.

[5] Thang, P.T., Nguyen, T.-T., Lee, J. (2017). A new approach for nonlinear buckling analysis of imperfect functionally graded carbon nanotube-reinforced composite plates. *Composites Part B: Engineering*, vol. 127, p. 166-174, **DOI:10.1016/j.compositesb.2016.12.002**.

[6] Ashoori, A.R., Salari, E., Sadough Vanini, S.A. (2016). Size-dependent thermal stability analysis of embedded functionally graded annular nanoplates based on the nonlocal elasticity theory. *International Journal of Mechanical Sciences*, vol. 119, p. 396-411, **DOI:10.1016/j.ijmecsci.2016.10.035**.

[7] Challamel, N., Hache, F., Elishakoff, I., Wang, C.M. (2016). Buckling and vibrations of microstructured rectangular plates considering phenomenological and lattice-based nonlocal continuum models. *Composite Structures*, vol. 149, p. 145-156, **DOI:10.1016/j.compstruct.2016.04.007**.

[8] Liu, J.C., Zhang, Y.Q., Fan, L.F. (2017). Nonlocal vibration and biaxial buckling of double-viscoelastic-FGM-nanoplate system with viscoelastic Pasternak medium in between. *Physics Letters A*, vol. 381, no. 14, p. 1228-1235, **DOI:10.1016/j.physleta.2017.01.056**.

[9] Golmakani, M.E., Rezatalab, J. (2015). Nonuniform biaxial buckling of orthotropic nanoplates embedded in an elastic medium based on nonlocal Mindlin plate theory. *Composite Structures*, vol. 119, p. 238-250, **DOI:10.1016/j.compstruct.2014.08.037**.

[10] Taati, E. (2018). On buckling and post-buckling behavior of functionally graded micro-beams in thermal environment. *International Journal of Engineering Science*, vol. 128, p. 63-78, **DOI:10.1016/j.ijengsci.2018.03.010**.

[11] Ebrahimi, F., Barati, M.R. (2017). Buckling analysis of nonlocal strain gradient axially functionally graded nanobeams resting on variable elastic medium. *Proceedings of the Institution of Mechanical Engineers, Part C: Journal of Mechanical Engineering Science*, vol. 232, no. 11, p. 2067-2078, **DOI:10.1177/0954406217713518**.

[12] Ebrahimi, F., Shaghaghi, G.R., Boreiry, M. (2016). A semi-analytical evaluation of surface and nonlocal effects on buckling and vibrational characteristics of nanotubes with various boundary conditions. *International Journal of Structural Stability and Dynamics*, vol. 16, no. 6, p. 1550023, **DOI:10.1142/S0219455415500236**.

[13] Latifi, M., Farhatnia, F., Kadkhodaei, M. (2013). Buckling analysis of rectangular functionally graded plates under various edge conditions using Fourier series expansion. *European Journal of Mechanics - A/Solids*, vol. 41, p. 16-27, **DOI:10.1016/j.euromechsol.2013.01.008**.

[14] Pradhan, S.C., Murmu, T. (2010). Small scale effect on the buckling analysis of single-layered graphene sheet embedded in an elastic medium based on nonlocal plate theory. *Physica E: Low-dimensional Systems and Nanostructures*, vol. 42, no. 5, p. 1293–1301, **DOI:10.1016/j.physe.2009.10.053**.

[15] Shahidi, A.R., Anjomshoa, A., Shahidi, S.H., Kamrani, M. (2013). Fundamental size dependent natural frequencies of non-uniform orthotropic nano scaled plates using nonlocal variational principle and finite element method. *Applied Mathematical Modelling*, vol. 37, no. 10-11, p. 7047-7061, **DOI:10.1016/j.apm.2013.02.015**.

[16] Asbaghian Namin, S.F., Pilafkan, R. (2017). Vibration analysis of defective graphene sheets using nonlocal elasticity theory. *Physica E: Low-dimensional Systems and Nanostructures*, vol. 93, p. 257-264, **DOI:10.1016/j.physe.2017.06.014**.

[17] Zhang, L.W., Zhang, Y., Liew, K.M. (2017). Vibration analysis of quadrilateral graphene sheets subjected to an in-plane magnetic field based on nonlocal elasticity theory. *Composites Part B: Engineering*, vol. 118, p. 96-103, **DOI:10.1016/j.compositesb.2017.03.017**.

[18] Li, L., Hu, Y. (2017). Torsional vibration of bi-directional functionally graded nanotubes based on nonlocal elasticity theory. *Composite Structures*, vol. 172, p. 242-250, **DOI:10.1016/j.compstruct.2017.03.097**.

[19] Demir, Ç, Civalek, O. (2017). A new nonlocal FEM via Hermitian cubic shape functions for thermal vibration of nano beams surrounded by an elastic matrix. *Composite Structures*, vol. 168, p. 872-884, **DOI:10.1016/j.compstruct.2017.02.091**.

[20] Murmu, T., Adhikari, S. (2011). Nonlocal vibration of bonded double-nanoplate-systems. *Composites Part B: Engineering*, vol. 42, no. 7, p. 1901-1911, **DOI:10.1016/j.compositesb.2011.06.009**.

[21] Trefethen, L.N. (2000). *Spectral Methods in MATLAB, Software, Environments, and Tools*. SIAM, Philadelphia, **DOI:10.1137/1.9780898719598**.

[22] Shahba, A., Rajasekaran, S. (2012). Free vibration and stability of tapered Euler–Bernoulli beams made of axially functionally graded materials. *Applied Mathematical Modelling*, vol. 36, no. 7, p. 3094-3111, **DOI:10.1016/j.apm.2011.09.073**.

[23] Pradhan, S.C., Murmu, T. (2009). Thermo-mechanical vibration of FGM sandwich beam under variable elastic foundations using differential quadrature method. *Journal of Sound and Vibration*, vol. 321, no. 1-2, p. 342-362, **DOI:10.1016/j.jsv.2008.09.018**.

[24] Reddy, J.N. (2007). Nonlocal theories for bending, buckling and vibration of beams. *International Journal of Engineering Sciences*, vol. 45, no. 2-8, p. 288-307, **DOI:10.1016/j.ijengsci.2007.04.004**.